Surface Modification of Cotton Gauze by Silk Fibroin Nanofibers as Compatible Biomaterial

A. Zare

Department of Textile Engineering, Yazd University, P.O. Box: 8915818411, Yazd, Iran.

ABSTRACT

*T*he present research explores preparing and characterizing silk fibroin electrospun nanofibers on cotton gauze bandages to form a novel silk-gauze nanocomposite. The presence of the extracted silk fibroin on the cotton substrate surface was demonstrated by scanning electron microscopy (SEM), attenuated total reflectance Fourier transform infrared spectrophotometry (ATR-FTIR), wide-angle X-ray diffraction (WAXD) and K/S values. The SEM images of cotton samples revealed the deposition of silk fibroin from silk fiber on the substrate surface. The dyed silk-gauze nanocomposite wound dressing presented significantly higher color strength than an uncoated gauze bandage. The physical properties of nanocomposite samples, i.e., porosity, tensile strength, bending characterizations, air permeability, and water uptake, were measured. The changes in the secondary structure of silk fibroin, morphology, crystallinity, hydrophilicity as well as cytotoxicity of nanocomposites were analyzed before and after undergoing treatments with ethanol and methanol. The results demonstrated a decrease in water uptake and porosity values and a slight increment in tensile strength and bending characterization of the treated nanocomposite samples compared to the untreated samples. MTT assay as an indirect cytotoxicity method showed cytocompatibility of the silk-gauze nanocomposite wound dressing. The indirect cytotoxicity results showed that samples treated with ethanol demonstrated no cytotoxicity on the L929 cancer cell line. Prog. Color Colorants Coat. 18 (2025), 163-176© Institute for Color Science and Technology.

1. Introduction

Biopolymers such as polynucleic acids, polysaccharides, polyamino acids, and polyphenols have evolved over billions of years to carry out myriad tasks such as storing energy, molecular recognition, or catalysis [1, 2]. Silk is a well-known textile fiber aptly known as the "Queen of Textiles" for its luxury, appeal, elegance, comfort, luster, glamour, and sensuousness. Silk possesses exceptional qualities comparable to other synthetic polymers; however, its production does not necessitate harsh processing conditions [3]. The primary components of raw silk fibers consist of two main proteins: fibroin, which makes up approximately 66 % by weight, and sericin, comprising around 26 % by weight. During the manufacturing processes in the textile industry, the sericin adhesive with impurities is eliminated from the thread through a degumming process [4]. The Bombyx mori silkworm's silk cocoons produce fibroin fibers that are highly coveted in the textile industry due to their velvety softness to the touch and lustrous sheen.These fibroin fibers can be conventionally fabricated into diverse forms, including non-woven fabrics, knitted garments, braided cords, and reinforcing matrices [5-8].

Silk fibroin (SF) has a combination of attractive machinability, controllable biodegradability, good biocompatibility, adsorption properties, hemostatic properties, permeability, non-cytotoxicity, microbial resistance, high thermal stability, good oxygen, and water vapor permeability, low antigenicity, noninflammatory characteristics, bioresorbability, etc. which make it a highly appreciated material in cosmetics, biomedical, pharmaceutical and textile industries [9-15]. It can be used as a biomaterial in various forms, such as membranes, films, powders, sponges, gels, and scaffolds. The versatile uses span a wide range, encompassing protective coverings for burn wounds, matrices that immobilize enzymes, systems for controlled drug delivery, netting materials, contact lenses for vision correction, artificial vascular grafts, and structural implants for the body [16-25]. Silk has been employed as a material for surgical sutures for many decades [8, 10].

Like other proteins, silk fibroin (SF) is a complex structure formed by various amino acids. These amino acids serve as cell receptors, enabling crucial interactions between mammalian cells and the extracellular matrix (ECM). This interaction facilitates cell adhesion and growth. Additionally, silk fibroin exhibits antimicrobial properties [11, 26]. Due to their influence on physical and chemical properties, the molecular conformation of SF membranes is an important parameter that needs to be controlled. Process conditions like drying temperature, solvent type, and solution concentration can be leveraged to control the molecular conformation within the SF substrate. Additionally, post-processing treatments play a defining role in establishing the secondary structure of SF materials [10].

Treatments by immersion and solvent vapor with organic low-dielectric solvents, such as methanol or ethanol, are commonly used to convert SF from random coil to β-sheet conformation. This treatment increases the crystallinity and improves the stability of the treated samples against water [10, 27]. As nanotechnological manufacturing techniques advance, biotextiles are finding novel applications. With the development of nanotechnological manufacturing technologies, new usages for biotextiles have been recognized. Combiningbiotextile technology and nanotechnology has yielded a new field in areas such as bandages, tissue scaffolds, and wound dressings [12].

Recently, wound dressings utilizing bionanofibers have shown remarkable versatility and functionality. These dressings exhibit characterizations such as oxygen permeability, excellent wound adherence, resorbability, absorption capabilities, and occlusivity. Due to their high surface area-to-volume ratios, nanofiber webs can effectively filter contaminants, microorganisms, and particulates. Additionally, they can function as controlled drug-release matrices. The unique properties of nanofibers make them well-suited for biomedical applications. Their highly porous network, with interconnected pores, facilitates the essential pathways for nutrient delivery and oxygen transport crucial for cellular growth and tissue regeneration [28-31]. Martindale and coworkers highlighted the potential of electrospun wound dressings in minimizing scarring and promoting healthy skin regeneration. Despite their efficacy, the broad utilization of nanofiber webs in wound dressings has been constrained by challenges related to their mechanical characteristics and handling complexities [32-34].

Sterilization is crucial for materials or devices intended for use as biomaterials. While ethanol treatment is commonly used as a disinfectant, it is not considered a sterilization method because it does not effectively eliminate endospores from most bacterial species, thus restricting its efficacy as a surface-sterilizing agent. Despite this limitation, ethanol treatment remains widely employed as a disinfection method for various materials [35].

This study aims to produce silk-gauze nano-composite wound dressings. In this research, the nanocomposite bandages were formedby electrospinning SF nanofiber onto 100 % cotton gauze substrates. The effect of ethanol and methanol treatments on the nano-composite gauze bandage properties wasinvestigated. The raw bandage's and untreated and treated mats' physical and mechanical properties, such as tensile strength, bending characterizations, andwater uptake, were determined. The chemical, morphology, and crystallinity of nanocomposites, as well as the changes in the secondary structure of silk fibroin, were analyzed before and after treatment with ethanol and methanol by infrared spectroscopy with attenuated total reflection (FTIR-ATR), scanning electron microscopy (SEM) and X-ray diffraction pattern (XRD) techniques, respectively. The dyeability of samples was investigated by dyeing with acid dye. Also, the cytotoxicity analysiswasdone by L929 fibroblasts with MTT assay.

2. Experimental

2.1. Materials

Raw cocoons of the silkworm, Bombyx mori were purchased from a silk company (Rasht, Iran). Solvent impurities from silk fibroin solution were removed using cellulose dialysis cassettes (Slide-A-lyzer molecular, weight cutoff 3500 (Pierce)). $CaCl_2$, Na_2CO_3, ethanol,and methanol were supplied by Merckand used as received. Other chemicals used were pharmaceutical or analytical grade and purchased from Sigma–Aldrich or Merck. L929 fibroblast cells were preparedby the Ministry of Food, Agriculture and Livestock.

2.2. Preparation of silk fibroin (SF) solution

The cocoons were degummed thrice in an aqueoussolution of 0.02 M Na_2CO_3 at 85 °C for 30 min to remove the sericin proteins. The fibers were then rinsed with water and dried at room temperature. The resulting fibers were then dissolved in a ternary solvent of $CaCl_2$: CH_3CH_2OH: H_2O (1:2:8 molar) at 85 °C until total dissolution and formed a yellow viscose solution. This solution was dialyzed against distilled water using cellulose dialysis cassettes for 3 days to remove the salt.

The solution was optically clear after dialysis and was centrifuged at 8000 rpm for 10 min to remove the small amount of silk aggregates that formed during the process. Then, the aqueous SF solution was dried at room temperature. The SF/ trifluoroacetic acid (TFA) solution was prepared by dissolving the SF in TFA for 12 h.

2.2. Electrospinning and treatment

2.2.1. Electrospinning of nanofiber mats onto fabric

SF nanofibers were electrospun using an electrospinning apparatus with a rotating drum for collection. Electrospunnanofibers were collected on the cotton gauze bandage for 30, 60, 120, and 180 minutes. The electrospinning was performed at room temperature. To obtain smooth and uniform fibroin nanofibers, the main processing parameters,such as the flow rate of the feedstock, the distance between the tip and collector, and applied electric field syringe were set constant (flow rate: 0.2 mL/h, distance: 12 cm, voltage: 30 kV). In this article, fibroin was dissolved at a concentration of 12 % (w/v) in TFA.

2.2.2. Ethanol and methanol treatments

To undergo structural change from amorphous to β-sheet conformation, crystallization, and sterilization to form as-spun SF electrospun fiber insoluble in water,It was immersed 15 min in methanol and 15 min in ethanol, then dried at room temperature for 36 hours.

2.3. Characterization

2.3.1. Evidence of silk fibroin nanofiber deposition on the cotton gauze bandage

The uncoated, untreated, and treated bandage samples were dyed with 1 % W/V aqueous solution of acid dye Telon Red 51 under acidic conditions (pH 4.5) at a liquor-to-fabric ratio of 40:1 for 45 min at 85 °C, in an infrared dyeing machine (D400IR- Ahiba, England). The UVmini-1240 spectrophotometer was used to measure the reflectance of the dyed samples over the 400-700 nm range. The color strength (K/S) was determined by applying the Kubelka-Munk equation, represented by equation 1.

$$\frac{K}{S} = \frac{(1-R)^2}{2R} \tag{1}$$

K/S is color strength, and R is the maximum reflectance of the cotton fabrics [36].

2.3.2. Physical and chemical property tests of nanofiber mats and silk-gauze nanocomposite samples before and after treatment

To visualize the nanofibers, they were first coated with a thin layer of gold using a sputtering process. This gold coating enhances the conductivity of the sample, allowing for better imaging under the scanning electron microscope (SEM). The SEM images of these gold-sputtered nanofibers were then acquired using a Vega 3 Tescan-SB microscope operating at an accelerating voltage of 20 kilovolts (kV). The fiber diameters were measured using SEM software, and a statistical analysis was conducted on 50 randomly selected fiber samples.

The pore size and air permeability of electrospun nanofiber mats play an essential role in the successful applications of many nanofiber mats. Enhancing the performance of nanofiber-based materials in biomedical applications depends on the porous structure of nanofiber mats [31]. To calculate the samples' porosity, a

MATLAB program was developed so that the empty and fiber spaces were considered 0 and 1, respectively. Consequently, the number of 0 values determines the porosity of the sample, as shown in equation 2.

$$\text{Porosity (\%)} = \frac{\text{The number of 0 values}}{\text{the size of the sample in pixels}} \times 100 \qquad (2)$$

FTIR spectra of the raw gauze bandage (control sample), as-spun,and treated nanofiber mats were shown using the FTIR Equinox 55 spectrometer (Germany) in the 4000–400 cm^{-1} wavenumber.

Wide-angle X-ray diffraction (WAXD) patterns were recorded on anAsenware model XDM300-AW diffractometer with CuKα radiation (λ=1.54 Å) at a scan rate of 1°/s within the scanning region of 2θ=5–30° at 40 kV and 30 mA.

The mechanical properties of the electrospun nanofiber mats onto the cotton gauze bandages (dimensions of 3 × 1 cm) before and after treatments were recorded using a Shirley micro 350 fiber tensile tester at environment conditions. The gauge length was constant at 2 cm, and thestrain rate was 10 mm/min. At least 5 samples were tested, and their load-strain curves were recorded. The results of the tensile strengthswereaveraged and reported.

The concept of "bending stiffness" is a significant factor in assessing fabric handles, representing the garment's ability to resist bending when subjected to external forces [38]. The bending stiffnessof the various gauze bandage sampleswere also calculated using equation 3.

$$G = 9.8 \times M \times (C)^3 \times 10^{-3} \qquad (3)$$

In this equation, G, M, and C represent the bending stiffness (in μN.m), fabric weight (in g/m^2), and average bending length (in cm), respectively. The fabric bending length was measured using the ASTM D 1388-96 (2002) testmethod [37].

The air permeability of a fabric specimen indicates the extent to which air can pass through it [38]. The air permeability of the samples was measured using Airpermeability tester M021(Shirley, England). Samples measuring 5 × 5 cm were cut from the nanofiber mats, and the air permeability of each sample was measured at an air pressure of 1 bar. A minimum of 5 samples were examined, and the average results were documented. The percentage of water uptake in the control, untreated, and treated silk-gauze nanocomposite samples was

reported. The 4 × 4 cm cotton gauze samples were soaked in distilled water for 24 hours, following which any extra water was eliminated. The damp fabrics were weighed, subjected to drying at 110 °C for 120 minutes in an oven, and then weighed again. The water absorption percentage was calculated using equation 4 [36].

Water uptake

$$(\%) = \frac{\text{Weight of wet fabric-Weight of dried fabric}}{\text{Weight of dried fabric}} \times 100 \qquad (4)$$

The MTT assay was conducted to evaluate cell viability and mitochondrial activity. The cytotoxicity of the silk-gauze nanocomposite samples was assessed following the ISO10993-5 standard test method for indirect contact. Statistical analysis was carried out using SPSS v.16.0 software, and the results were documented as mean values with standard deviations.

3. Result and Discussion

3.1. Evidence of silk fibroin presence on cotton gauze bandages

The impact of silk fibroin nanofibers on both the as-spun and treated cotton samples was examined. Following the dyeing process, the reflectance of the cotton gauze samples was measured, and the color strength (K/S) was calculated. Figure 1 illustrates that the K/S value for the sample coated with nanofiber mats during a 180-minute electrospinning period is 7.4, in contrast to 0.6 for the untreated sample. This outcome indicates a higher presence of amino groups from silk fibroin on the surface of the cotton gauze sample as the electrospinning time increases. When subjected to dyeing in an acidic environment, these amino groups exhibited a positive charge, enhancing ionic attraction and consequently boosting the absorption of acid dye [38]. The treatment of nanocomposite samples with ethanol or methanol decreases K/S valuesdue to the increasing hydrophobic nature of nanofibers and the decreasing porosity of formed mats onto cotton gauze bandages (Figure 2). However, Figure 2 shows that the K/S values of the treatment of nanocomposite samples with ethanol or methanol are almost the same, and increasing the electrospinning period has not affected the color strength of coated samples.
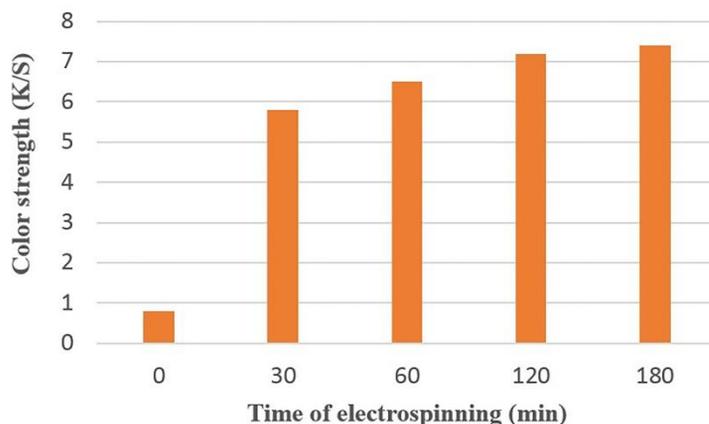
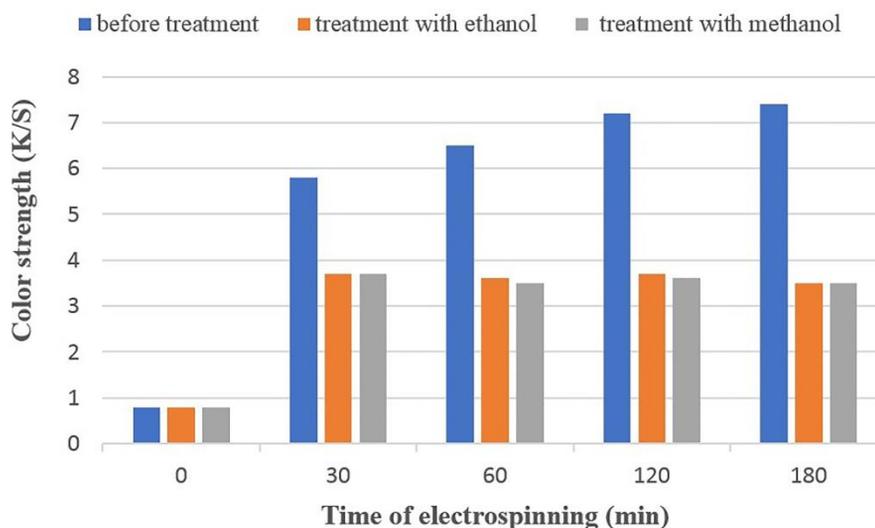**Figure 1:** Color strength of coated samples by silk fibroin nanofibers before treatment.

Figure 2: The relationship between color strengthin dyed cotton fabrics as a function of time of electrospinning before and after treatment with ethanol and methanol.

3.2. SEM

The SEM images in Figure 3 display the control, as-spun, and treated samples. As illustrated in Figure 3, the silk fibroin nanofibers were observed to be deposited onto the surface of the cotton bandage. Also, treatment with ethanol and methanol increases the diameter average of nanofibers. The evidence obtained through SEM imaging agrees with the findings of the previous testing. SEM observations (Figures 3b and 3c) did not show morphological changes in the silk-gauze nanocomposite after treatment with ethanol and methanol. Also, theresults show that the time of electrospinning had no significant effect on the average diameter of mats (Table 1). These findings confirm that the spinning time and the treatment with methanol and ethanol did not significantly affect the morphology of the samples.

The results presented that treatment with ethanol and methanol causes a contraction in the protein material due to molecular interactions between the polar solvent and the protein chains, which causes a reduction in the porosity of materials treated with these alcohols and increased surface wrinkles [39, 40] (Table 2).

Moreover, the hydrophobic molecular chains in the random coil configuration facilitate the formation of a compact crystal nucleus. This process involves reorganizing hydrogen bonds, promoting the development of a stable beta-sheet structure. The reconfiguration of hydrogen bonds leads to the expulsion of water, enhancing the stability of β-sheets and causing a reduction in porous structures following treatments with ethanol and methanol [41].
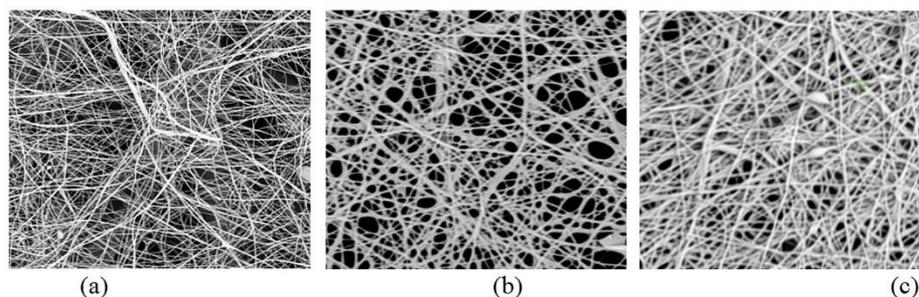
Figure 3: (a) as-spun silk fibroin nanofiber mats and (b) treated by ethanol and (c) methanol.

Table 1: Summary of the value average diameter.

Time of electrospinning (min)	Average diameter of samples before treatment (nm)	Average diameter of samples treated with ethanol (nm)	Average diameter of samples treated with methanol (nm)
0	-	-	-
30	490±40	536±33	561±42
60	489±44	538±41	560±29
120	491±45	539±37	566±51
180	493±43	541±35	566±45

Table 2: Summary of the porosity percentages.

Time of electrospinning (min)	Average porosity of as-spun samples (%)	Average porosity of samples treated by ethanol (%)	Average porosity of samples treated by methanol (%)
0	36	36	36
30	28	21	22
60	22	15	14
120	18	12	12
180	15	11	10

3.3. ATR-FTIR

ATR-FTIR spectroscopy was utilized to analyze the conformational and secondary structure alterations in silk fibroin following treatment with methanol and ethanol. The results gathered using Fourier transform infrared spectroscopy (FTIR) showed a difference between the cotton gauze samples before and after the treatment (Figure 4). The major bands of the cotton bandage are OH stretching, placed around 3324 cm^{-1}, CH stretching around 2830 cm^{-1}, CH$_2$ symmetric stretching near 1430 cm^{-1}, CH stretching placed around 1316 cm^{-1}, CO stretching around 1050 cm^{-1}, and a C−O−C non-symmetric bond placed around 1238 cm^{-1}. Figure 4b shows the FTIR spectrum of the as-spun silk fibroinfibers coated on the cotton bandage.

The spectral data presented in this image displays prominent absorption bands at specific wavenumbers: 1654 cm^{-1} (assigned to amide I), 1522 cm^{-1} (assigned to amide II), and 1202 cm^{-1} (assigned to amide III). These bands are indicative of the random coil conformation of silk fibroin. To gain a more detailed understanding of the conformation of electrospun silk fibroin, FTIR spectroscopy was employed on the treated mats. Figure 1c exhibits the FTIR spectra of silk fibroin fibers post-treatment with methanol for 180 minutes. Unlike the untreated nanofibers, both methanol and ethanol-treated mats exhibit absorption bands at 1637 cm^{-1} (amide I), 1480 cm^{-1} (amide II), and 1240 cm^{-1} (amide III), which are associated with theβ-sheet conformation of silk fibroin.

The absorption bands in the FTIR spectra of samples treated with methanol and ethanol are remarkably alike, indicating a similar mechanism of conformational changes in silk fibroin during treatment. The observed behavior stems from converting random coil structures into β-sheets following the treatments administered [42-44]. The crystallinity index (CI) of the as-spun and treated samples was calculated using equation 5 [27].

$$\text{Crystallinity index (CI)} = \frac{A_{1620\text{cm}^{-1}}}{A_{1645\text{cm}^{-1}} + A_{1620\text{cm}^{-1}}} \times 100 \qquad (5)$$

Methanol and ethanol are commonly recognized as effective agents for crystallizing silk fibroin molecules.

The proposed mechanism for crystallization involves the dehydration of protein materials during treatment, driven by their polar nature, which encourages the aggregation of hydrophobic amino acids. The phenomenon induces a strong interaction between amino acids, facilitating the molecular structure's reordering. This leads to a transition from random spiral conformations to β-sheet conformations [45-47]. These results indicate that compared with as-spun SF nanofiber mats, treated SF nanofiber mats seem to have higher crystalline content with more β-sheet conformations and lower presence of amorphous structures like random coil (Table 3).

Table 3: CIof samples after treatment with ethanol and methanol calculated from the FTIR spectrum.

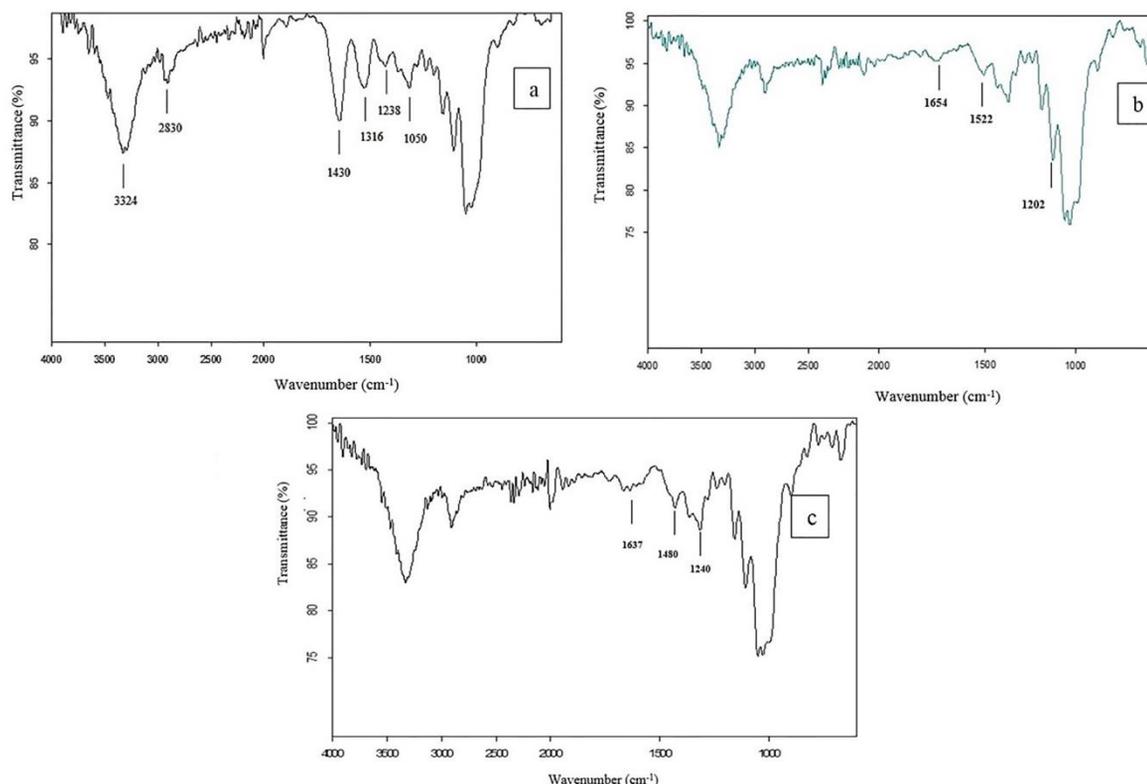| Time of electrospinning (min)	CI of treated samples by ethanol (%)	CI of treated samples by methanol (%)
0	-	-
30	32	33
60	32	32
120	32	33
180	32	33

Figure 4: ATR-FTIR spectra of cotton fabric samples (a) uncoated cotton bandage (control sample),(b) cotton bandage coated by fibroin nanofibers, (c) cotton bandage coated by fibroin nanofibers and treated with methanol.

3.4. Wide angle X-ray diffraction (WAXD)

To explore changes in the structure of electrospun silk fibroin following ethanol and methanol treatments, a WAXD analysis was performed. Figure 5 illustrates the X-ray findings for the as-spun fibers and those treated with methanol and ethanol. Consistent with the FTIR results, the X-ray diffractogram of the as-spun nanofibers shows minimal peaks indicative of crystalline organization, aligning with the FTIR data. Conversely, the nanofibers treated with methanol and ethanol exhibit three distinct diffraction peaks at $2\theta = 14$, 17, and 23, corresponding to β-sheet crystalline spacings of 10.3, 4.5, and 3.8 Å, respectively [48]. The XRD crystallinity of the treated electrospun fibers with ethanol and methanol was determined by calculating the ratio of the crystalline peak area to the total area in the diffractograms, as detailed in Table 4.

The findings confirm that the crystallinity of the samples undergoes an increase following treatment with ethanol and methanol. Immersion of all samples in ethanol or methanol demonstrates a notable trend towards heightened diffraction intensity, indicative of a reorganization into a more structured array. These outcomes align with the conformational transition mechanisms reported by previous researchers, which involve the development of highly ordered and stable β-sheets while decreasing the presence of random coil and less ordered β-sheet characteristics [49]. The emergence of a second band can be attributed to a molecular contraction within the fibroin structure, resulting in a shrinkage of the protein lattice parameters due to the well-established hydrophilic nature of the protein [14]. Furthermore, the transformation of random structures into β-sheets contributes to an increased orderliness of the protein, as documented in existing literature.

The crystallinity levels of fibers treated with methanol and ethanol closely align with predictions from IR spectroscopy. Discrepancies arise between the crystallinity values obtained from XRD and IR spectroscopy due to their sensitivity to different structural orders. IR spectroscopy primarily captures short-range order, while X-ray diffractometry focuses on larger-range order [50]. Consequently, X-ray diffractograms yield lower crystallinity values than IR spectroscopy since XRD detects mainly interplanar spacing of crystallites.
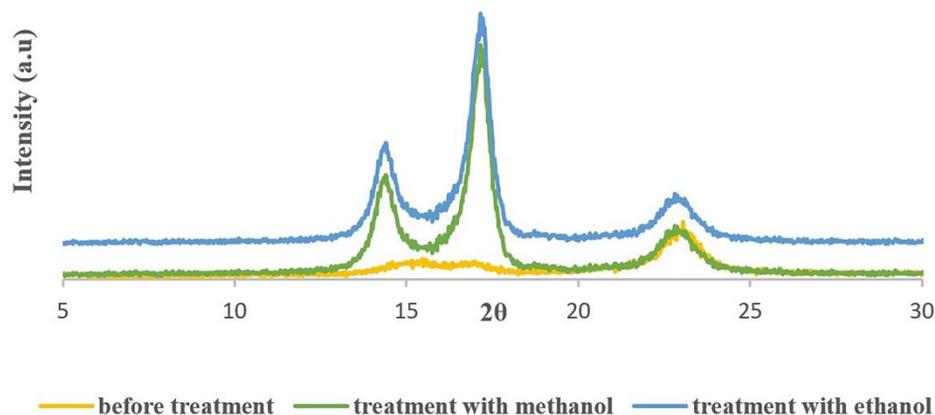

Figure 5: X-ray diffraction patterns of silk nanofiber mats produced by electrospinning: Untreated, treated with methanol, and treated with ethanol.

Table 4: Crystallinity of samples after treatment by ethanol and methanol calculated from XRD curves.

Time of electrospinning (min)	CI of treated samples by ethanol (%)	CI of treated samples by methanol (%)
0	-	-
30	32	33
60	32	32
120	32	33
180	32	33

3.5. Tensile properties

The results in Table 5 display the tensile strength values for the control, as-spun, and treated nanofiber mats. The findings reveal that treating the nanofiber mats with methanol and ethanol increased tensile strength. This finding suggests that the treated nanofiber mats exhibit a tougher, brittle, and stronger structure. Additionally, the data indicates that changing the electrospinning time did not significantly impact the tensile strength results of the samples.

3.6. Bending length and bending stiffness of samples

After conducting tests, the initial bending length of the raw cotton gauze bandage measures 1.7 cm. Subsequent coating processes result in an observed increase in bending length, as illustrated in Figure 6. Figure 7 demonstrates that the stiffness of the silk-gauze nanocomposite is enhanced due to the SF nanofiber coating, which increases tangential sliding resistance at the warp and weft interlacing points, consequently increasing bending stiffness. This approach elevates the fabric's stiffness and enhances its crease recovery capabilities [51].

Table 5: Tensile strength of silk nanofiber mats before and after treatment with ethanol and methanol.

Time of electrospinning (min)	Tensile strength of samples before treatment with ethanol and methanol (MPa)	Tensile strength of samples treated with ethanol (MPa)	Tensile strength of samples treated with methanol (MPa)
0	35.4[a] ±8.4	42.2±5.2[b]	40.8±6.0
30	36.4±10.5	43.0±8.2	42.7±8.4
60	36.8±12.4	44.1±6.8	44.1±7.3
120	37.1±8.9	44.5±4.5	44.3±5.0
180	37.2±7.1	44.9±11.0	45.1±11.1

a) Mean value of ultimate tensile strength; b) Standard deviation of ultimate tensile strength
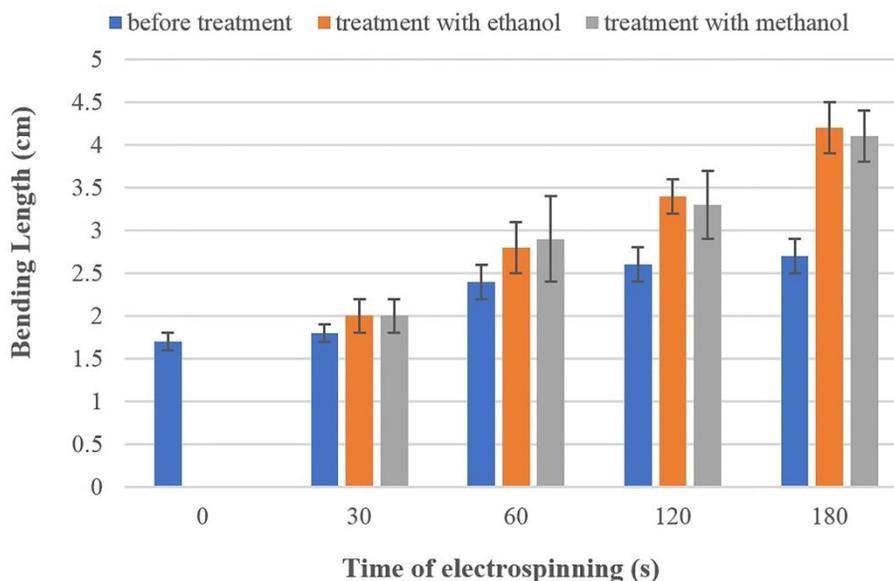

Figure 6: Bending length of the control, as-spun, and treated samples by ethanol and methanol treatment.
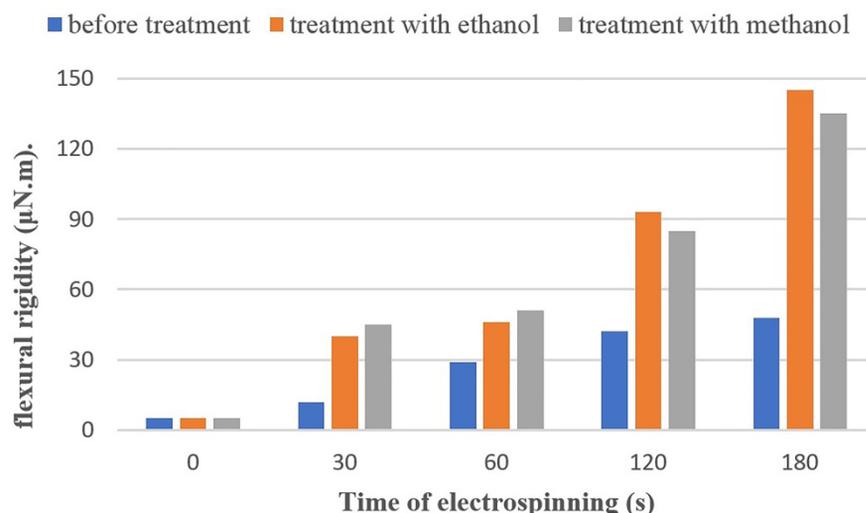
Figure 7: Bending stiffness of samples as a function of time of electrospinning before and after ethanol and methanol treatment.

3.7. Air permeability

The air permeabilities of the substrate materials with and without SF nanofibersare summarized in Figure 8. The cotton gauze bandage without SF nanofibers exhibited an air permeability of 55 cc/s.cm^2, and the air permeability of substrates coated and treated with SF nanofibers demonstrated reduced air permeabilities. This reduction in air permeability is beneficial for wound healing as it helps maintain a moist environment [35]. The study indicates that the air permeability of the mats slightly decreases with longer electrospinning times of silk-gauze nanocomposites. Compared to wounds left exposed to air for healing, wounds covered by nanofiber mats exhibit a faster rate of epithelialization.

3.8. Water uptake capacity

Effective wound healing relies on proper moisture control, where an optimal balance is crucial. Excessive moisture trapped in the bandage can lead to maceration, while insufficient moisture can cause desiccation, hindering healing. Air permeability, water absorbency, and moisture vapor transmission are key in moisture management. When considering silk fibroin mate as a dressing for wound care, characteristics like swelling and moisture absorption capacity become significant. These properties should support the removal of excess exudates while ensuring a moist environment at the wound site to facilitate healing [52].
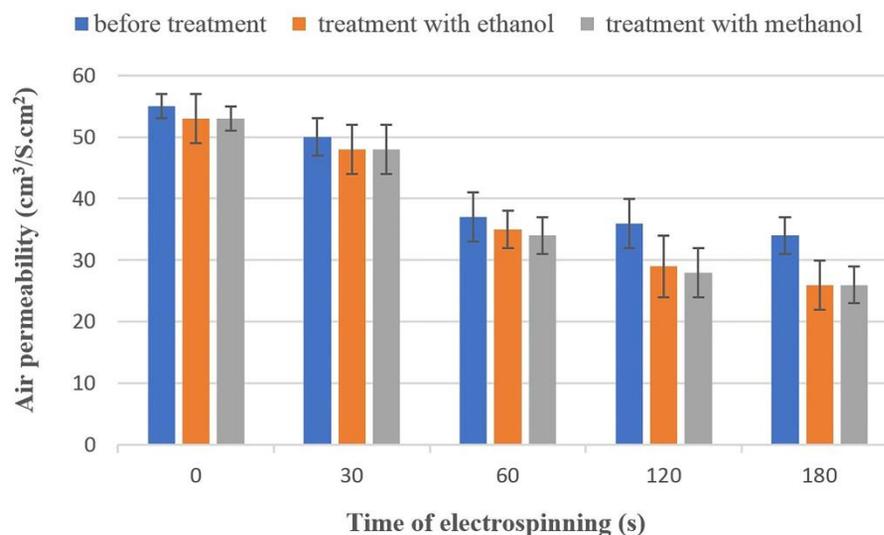

Figure 8: Air permeability of control, as-spun and treated cotton gauze bandage as a function of time spinning.

These results from Figure 9 confirm that the coating of bandage with fibroin nanofiber mats decreases hydrophilic properties. Fibroin, which contains hydrophobic amino acid residues like alanine, is insoluble in water, reducing the coated samples' hydrophilicity [54]. The exposure to ethanol and methanol treatments generates a change in the crystallinity of the sample. A possible mechanism of treatment action isthe expansion of the amorphous region of the proteins due to the interruption of hydrogen bonds in proteins. This behavior is followed by the penetration of ethanol and methanol into the expanded region to create a hydrophobic environment [53].

3.9. MTT assay

Treating silk fibroin nanofiber mats with methanol altered their microarchitecture and physicochemical characteristics but did not enhance cell viability. Conversely, ethanol-treated mats exhibited non-toxic properties towardcells, maintaining cell viability at 100%, comparable to the negative control (Figure 10).
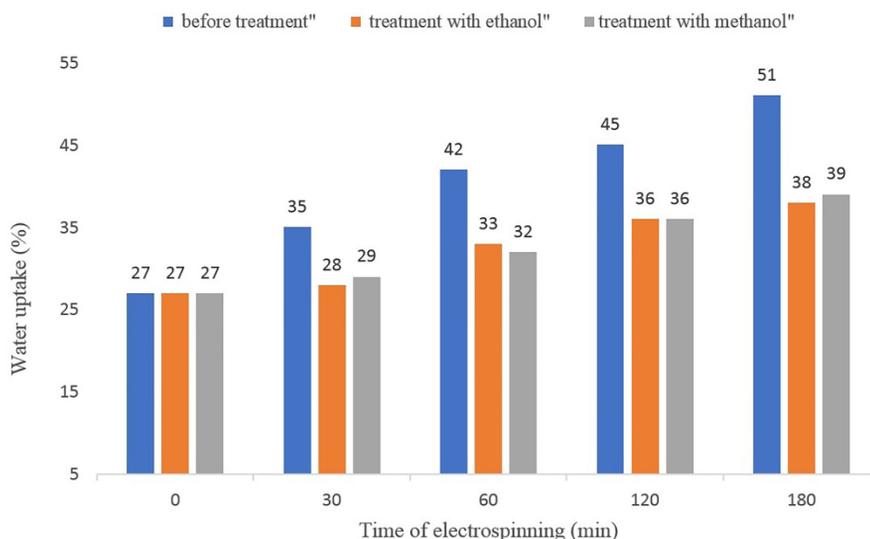

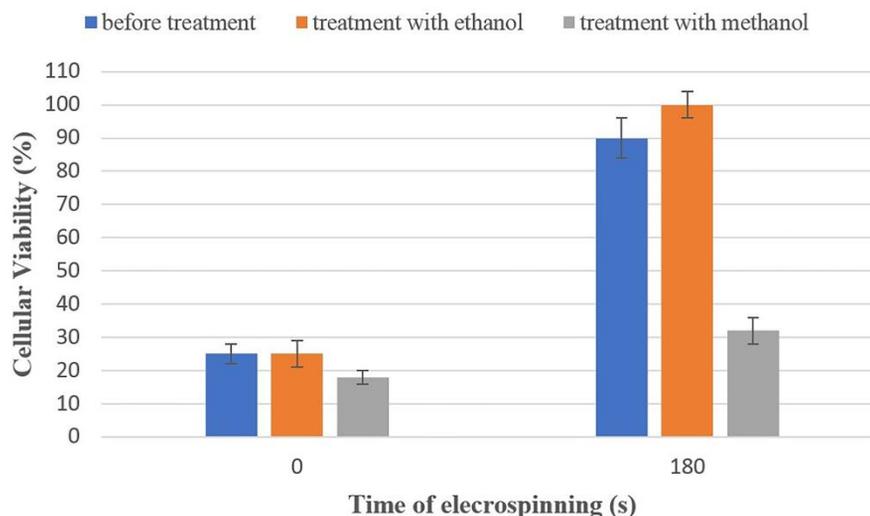**Figure 9:** Water uptake of samples.

Figure 10: The viability of human epithelial fibroblast cells was assessed after exposure to excipients derived from both untreated and treated stainless steel materials for 24 hours. A cellular control (CC) consisting of epithelial fibroblasts without any treatment was included for comparison.

4.Conclusion

This research involved electrospinning to treat cotton gauze bandages with fibroin, a protein extracted from silk cocoons.The successful fabrication of silk fibroin nanofiber mats with adjustable morphology and thickness was achieved by electrospinning silk fibroin solutions in TFA solvent at a concentration of 12 wt.%. The morphology and thickness of these mats can be controlled primarily by varying the electrospinning time. The confirmation of silk fibroin on the treated bandage was verified through FTIR analysis, SEM imaging, and acid dyeing techniques.

The physical, mechanical, and biological properties of nanofibrous silk fibroin mats coated onto cotton gauze bandages using ethanol and methanol treatments were assessed to develop a novel silk-gauze nanocomposite. Treatment with ethanol and methanol increased the durability of SF nanofibers electrospun onto cotton gauze substrates. The Evidence obtained through SEM imaging confirms that the spinning time and the treatment with methanol and ethanol did not significantly affect the morphology of the samples. The FTIR and WAXD results confirm that the crystallinity of the samples increases after treatment with ethanoland methanol. These results agree with conformational transition mechanisms, which involve the formation of highly ordered and stable β-sheet, while random coil and less ordered β-turn features tend to decrease.

The deposition of nanofibers led to enhancements in wound moisture management properties, characterized by increased water absorption and lower air permeability.The mechanical test results validated that treating the mats with ethanol and methanol improved their tensile strength due to promoting the formation of a β-sheet structure. These treatments were found to reduce the porosity of the uniformly arranged nanofibers. Moreover, the ethanol treatment notably boosted the proliferation rate of the L929 cancer cell line in vitro experiments, demonstrating no detectable cytotoxic effects.The significance of this fact lies in its implication that silk-gauze nanocomposite can be utilized as a wound dressing material.These innovative composite bandages are anticipated to provide a cost-effective, high-performance solution as a viable alternative to advanced wound dressings.

5. References

1. Hardy JG, Romer LM, Scheibel TR. Polymeric materials based on silk proteins. Polymer. 2008; 49(20): 4309–4327.https://doi.org/10.1016/j.polymer. 2008.08.006.

2. Vepari Ch, Kaplan DL, Silk as a biomaterial. Prog Polym Sci. 2007; 32(8-9): 991-1007. https://doi.org/10.1016/j.progpolymsci.2007.05.013.

3. Padaki NV, Das B, Basu A. Advances in understanding the properties of silk. In: Baltes H, Fedder GK, Korvink JG. (eds). Advances in Silk Science and Technology. Elsevier Ltd., Vol. 2 Wiley-VCH, Weinheim, Germany; 2004.p.3-16.

4. Reizaba A, Costa C M, Pérez-Álvarez L, Vilas-Vilela JL, Lanceros-Méndez S.Silk Fibroin as Sustainable Advanced Material: Material Properties and Characteristics, Processing, and Applications. Adv Funct Mater. 2023; 33(3): 2210764.https://doi. org/10.1002/adfm.202210764.

5. Terada D, Yokoyama Y, Hattori S, Kobayashi H, Tamada Y. The outermost surface properties of silk fibroin films reflect ethanol-treatment conditions used in biomaterial preparation. Mater Sci Eng C. Mater Biol Appl.2016; 58:119-126. https://doi.org/10.1016/j.msec.2015.07.041.

6. Tao H, Amsden JJ, Strikwerda AC, Fan K, Kaplan DL, Zhang X, et al. Metamaterial silk composites at terahertz frequencies. Adv Mater. 2010; 22(32): 3527-3531. https://doi.org/10.1002/adma.201000412.

7. Koha LD, Cheng Y, Teng CP, Khina YW, Loh XJ, Tee SY, et al. Structures, mechanical properties and applications of silk fibroin materials. Prog Polym Sci, 2015; 46:86-110. http:// dx.doi.org/10.1016/ j. progpolymsci. 2015.02.001.

8. Cao Y, Wang B. Biodegradation of Silk Biomaterials. Int J Mol Sci. 2009; 10(4): 1514-1524. http://dx. doi:10.3390/ijms10041514.

9. Zhang Q, Yan S, Li M. Silk fibroin based porous. Mater. 2009; 2(4): 2276-2295. http://dx.doi: 10. 3390/ma2042276.

10. Nogueira GM, Rodas AC, Leite CA, Giles C, Higa OZ, Polakiewicz B, et al., Preparation and characterization of ethanol-treated silk fibroin dense membranes for biomaterials application using waste silk fibers as raw material. Bioresour Technol. 2010; 101(21): 8446-8451. http://dx.doi:10.1016/j.biortech. 2010. 06.064.

11. Barud H, Barud HD, Cavicchioli M, do Amaral TS, de Oliveira Junior OB, Santos DM, et al.,Preparation and characterization of a bacterial cellulose/silk fibroin sponge scaffold for tissue regeneration. Carbohydr Polym. 2015; 128:41-51. http://dx.doi.org/ 10.1016/j.carbpol. 2015.04.007.

12. Çalamak S, Erdoğdu C, Özalp M, Ulubayram K. Silk fibroin based antibacterial bionanotextiles as wound dressing materials. Mater Sci Eng C. 2014; 43:11-20. http://dx. doi.org/10.1016/j.msec.2014.07.001

13. Liu J, Xie X, Wang T, Chen H, Fu Y, Cheng X, et al. Promotion of wound healing using nanoporous silk fibroin sponges. ACS Appl Mater Interfaces. 2023; 15(10): 12696-12707. https://doi.org/10.1021/ acsami.2c20274.

14. Um IC, KweonH, Park YH, Hudson S. Structural characteristics and properties of the regenerated silk fibroin prepared from formic acid. Int J Biol Macromol. 2001; 29(2): 91-97. https://doi.org/10. 1016/ S0141-8130(01)00159-3.

15. Li L, Zhou L, Zhu J, Jian M, Zhang J. Superstrong and tough silk fibers cross-linked with functionalized graphene. Carbon. 2024; 226:119227. https://doi.org/ 10.1016/j.carbon.2024.119227.

16. Xing X, Han Y, Cheng H. Biomedical applications of chitosan/silk fibroin composites: A review. Int J Biol Macromol. 2023; 240: 124407. https://doi.org/10. 1016/j. ijbiomac.2023.124407.

17. Acharya C, Hinz B, Kundu SC. The effect of lactose-conjugated silk biomaterials on the development of fibrogenic fibroblasts. Biomaterials 2008; 29(35): 4665-4675. https://doi.org/10.1016/j.biomaterials. 2008. 08.033.

18. Acharya C, Ghosh SK, Kundu SC. Silk fibroin protein from mulberry and non-mulberry silkworms: cytotoxicity, biocompatibility and kinetics of L929 murine fibroblast adhesion. J Mater Sci Mater Med. 2008; 19: 2827-2836. https://doi.org/10.1007/s10856-008-3408-3.

19. Kundu J, Dewan M, Ghoshal S, Kundu SC., Mulberry non-engineered silk gland protein vis-a-vis silk cocoon protein engineered by silkworms as biomaterial matrices. J Mater Sci Mater Med. 2008; 19: 2679-289. http://dx. doi.org/10.1007/s10856-008-3398-1.

20. Tran HA, Hoang TT, Maraldo A, Do TN, Kaplan DL, Lim KS, Rnjak-Kovacina J., Emerging silk fibroin materials and their applications: New functionality arising from innovations in silk crosslinking. Mater Today. 2023; 65: 244-259. https://doi.org/10.1016/ j.mattod.2023.03.027.

21. Zhang Y, Sheng R, Chen J, Wang H, Zhu Y, Cao Z, et al. Silk fibroin and sericin differentially potentiate the paracrine and regenerative functions of stem cells through multiomics analysis. Adv Mater. 2023; 35(20): 2210517. https://doi.org/10.1002/adma. 202210517

22. Yu B, Li Y, Lin Y, Zhu Y, Hao T, Wu Y, et al. Research progress of natural silk fibroin and the application for drug delivery in chemotherapies. Frontiers Pharmacol. 2023; 13:1071868. https://doi. org/ 10.3389/fphar.2022.1071868.

23. Dalpra I, Freddi G, Minic J, Chiarini A, Armato U. De Novo engineering of reticular connective tissue in vivo by silk fibroin nonwoven materials. Biomaterials.

24. Yang S, Zhao C, Yang Y, Ren J, Ling S. The fractal network structure of silk fibroin molecules and its effect on spinning of silkworm silk. ACS Nano. 2023; 17(8): 7662-7673. https://doi.org/10.1021/acsnano. 3c00105.

25. Mauney JR, Nguyen T, GillenK, Kirker-Head C, Gimble JM, Kaplan DL, Engineering adipose-like tissue in vitro and in vivo utilizing human bone marrow and adipose-derived mesenchymal stem cells with silk fibroin 3D scaffolds. Biomaterials. 2007; 28(35): 5280-5290. https://doi.org/10.1016/j. biomaterials. 2007.08.017.

26. Uebersax L, Hagenmuller H, Hofmann S, Gruenblatt E, Müller R, Vunjaknovakovic G, et al. Effect of scaffold design on bone morphology in vitro. Tissue Eng. 2006; 12(12): 3417-3429. https://doi.org/10. 1089/ ten.2006.12.3417.

27. Fang Q, Chen D, Yang Z, Li M, In vitro and in vivo research on using Antheraeapernyi silk fibroin as tissue engineering tendon scaffolds. Mater Sci Eng C. 2009; 29(5): 1527-1534. https://doi.org/10.1016/j. msec.2008.12.007.

28. Arango1 MC, Osorio YM, Osorno JB, Parra SB, Alvarez López C, Effect of ethanol post treatments over sericin scaffolds for tissue engineering aApplications. J Polym Environ 2022; 31(5):1800-1811. https://doi.org/10.1007/s10924-022-02647-3.

29. Venugopal J, Ramakrishna S, Application of polymer nanofibers in biomedicine and biotechnology. Appl BiochemBiotechnol. 2005; 125: 147-157. https://doi. org/10.1385/abab: 125:3:147.

30. Duan YY, Jia J, Wang SH, Yan W, Jin L, Wang ZY. Preparation of antimicrobial poly (ε-caprolactone) electrospun nanofibers containing silver-loaded zirconium phosphate nanoparticles. J Appl Polym Sci. 2007; 106(2): 1208-1214. https://doi.org/ 10.1002/ app.26786.

31. Madhugiri S, Sun B, Smirniotis PG, Ferraris JP, Balkus JrKJ. Electrospun mesoporous titanium dioxide fibers. MicroporMesopor Mater. 2004; 69(1-2): 77-83. https://doi.org/10.1016/ j.micromeso. 2003. 12.023.

32. Amiraliyana N, Nouri M, Haghighat Kish M. Structural characterization and mechanical properties of electrospun silk fibroin nanofiber. Mat Polym Sci Ser A. 2010; 52(4): 407-412. https://doi.org/10.1134/ S0965545X10040097.

33. Martindale D, Biodegradable scaffolds give skin cells a better road map for self-repair Sci Biodegradable,. 2000; 283: 34-36. https://www.jstor.org/stable/ 26058782.

34. Pandey V, Sharma A, Sharma A, Kumari V. The role of silk as natural biomaterial in food safety. Food Biosci. 2024; 60:104538. https://doi.org/10.1016/j. fbio.2024.104538.

35. Nawalakhe R, Shi Q, Vitchuli N, Bourhamb M A, Zhang X , McCord M G. Novel atmospheric plasma

enhanced silk fibroin nanofiber/gauze composite wound dressings. J Fiber Bioeng Inform. 2012; 5(3): 227-242. https://doi.org/10.3993/jfbi09201201.

36. De Moraes MA, Weska RF, Beppu MM. Effects of sterilization methods on the physical, chemical, and biological properties of silk fibroin membranes. J Biomed Mater Res B Appl Biomater. 2014; 102(4): 869-876. https://doi.org/10.1002/jbm.b.33069

37. KosawatnakulS, NakpathomM, Bechtold T, Aldred AK, Chemical finishing of cotton fabric with silk fibroin and its properties. Cellulose Chem Technol. 2018; 52(1-2): 123-128.

38. Gholamzadeh L, ZareMehrjardi A., Bismuth (III) oxide (Bi$_2$O$_3$)/poly (vinyl alcohol) nanocomposite fiber coated polyester fabrics for multifunctional applications. Clean Technol Environ Policy, 2023, 24:1-10. https://doi.org/10.1007/s10098-023-02533-z.

39. Peng H, Yang C Q, Wang S. Nonformaldehyde durable press finishing of cotton fabrics using the combination of maleic acid and sodium hypophosphite. Carbohyd Polym. 2012; 87(1): 491-499. htps://doi.org/10. 1016/j.carbpol.2011.08.013.

40. Jang MJ, Um IC, Effect of sericin concentration and ethanol content on gelation behavior, rheological properties, and sponge characteristics of silk sericin. Eur Polym J. 2017; 93:761-774. https://doi.org/10. 1016/j.eurpo lymj.2017.03.048.

41. Aramwit P, Siritientong T, Kanokpanont S, Srichana T, Formulation and characterization of silk sericin-PVA scaffold crosslinked with genipin. Int J Biol Macromol. 2010; 47: 668-675. https://doi.org/10. 1016/j. ijbio mac.

42. Sahi AK, Varshney N, Poddar S, Gundu S, Mahto SK, Fabrication and characterization of silk fibroin-based nanofibrous scaffolds supplemented with gelatin for corneal tissue engineering. Cells Tissues Organs. 2021; 210(3): 173-194. https://doi.org/10.1159/ 00051 5946.

43. Cardenas T GA, Sanzana L JO, InoccentiniMEI LH. Synthesis and characterization of chitosan-PHB blends, Bol Soc Chil Quim. 2002; 47(4): 529-535. https://doi.org/10.4067/S0366-16442002000400025.

44. Li M, Ogiso M, Minoura N. Enzymatic degradation behavior of porous silk fibroin sheets. Biomaterials.

2003; 24(2): 357-365. https://doi.org/10.1016/S0142-9612(02)00326-5.

45. Chen X, Knight DP, Shao Z, Vollrath F., Regenerated bombyx silk solutions studied with rheometry and FTIR. Polymer 2001;42(25):09969-09974. https://doi.org/10.1016/S0032-3861(01)00541-9.

46. Zhang KH, Ye Q, Yan Z Y. Influence of post-treatment with 75% (v/v) ethanol vapor on the properties of SF/P(LLA-CL) nanofibrous scaffolds. Int J Mol Sci. 2012; 13(2): 2036-2047. https://doi.org/10.3390/ijms13022036.

47. Puerta M, Arango MC, Jaramillo-Quiceno N, Álvarez-López C, Restrepo-Osorio A. Influence of ethanol post-treatments on the properties of silk protein materials. SN Appl Sci. 2019; 1(11):1443. https://doi.org/10.1007/s42452-019-1486-0.

48. Ki CS, Kim JW, Oh HJ, Lee KH, Park YH, The effect of residual silk sericin on the structure and mechanical property of regenerated silk filament. Int J Biol Macromol. 2007; 41(3): 346-353. https://doi.org/ 10.1016/j.ijbiomac.2007.05.005.

49. Lamboni L, Gauthier M, Yang G, Wang Q., Silk sericin: a versatile material for tissue engineering and drug delivery. Biotechnol Adv. 2015;33(8),1855-1867. https://doi.org/ 10.1016/j.biotechadv. 2015. 10.014.

50. Weska RF, Vieira Jr WC, Nogueira GM, Beppu MM., Effect of freezing methods on the properties of lyophilized porous silk fibroin membranes. Mater Res. 2009; 12: 233-237. https://doi.org/10.1590/S1516 - 14392 00900. 02000 20.

51. Wu Q, He C, Wang X, Zhang S, Zhang L, Xie R, et al. Sustainable antibacterial surgical suture using a facile scalable silk-fibroin-based berberine loading system. ACS Biomater Sci Eng. 2021; 7(6): 2845-257. https://doi.org/10.1021/acsbiomaterials.1c00481.

52. Kamoun EA, Kenawy ER, Chen X., A review on polymeric hydrogel membranes for wound dressing applications: PVA-based hydrogel dressings. J Adv Res. 2017; 8(3): 217-233. https:// doi.org/10.1016/ j. jare. 2017.01.005.

53. Hossain KS, Ohyama E, Ochi A, Magoshi J, Nemoto N., Dilute-solution properties of regenerated silk fibroin. J Phys Chem B. 2003; 107(32): 8066-8073. https://doi.org/10.1021/jp022490i.